RNL/TM-2023/3109

Light Water Reactor Sustainability Program

Complete the first phase of the comprehensive characterization of repair welding performed on irradiated Ni alloy 182

M3LW-23OR0406015

September 2023
U.S. Department of Energy
Office of Nuclear Energy

RNL/TM-2023/3109

Materials Science and Technology Division

COMPLETE THE FIRST PHASE OF THE COMPREHENSIVE CHARACTERIZATION OF REPAIR WELDING PERFORMED ON IRRADIATED NI ALLOY 182

M3LW-23OR0406015

Jian Chen, Roger Miller, Zhili Feng
Oak Ridge National Laboratory

Jonathan Tatman, Benjamin Sutton, Gregory Frederick
Electric Power Research Institute

September 2023

Prepared by

OAK RIDGE NATIONAL LABORATORY
Oak Ridge, TN 37831-6283
managed by
UT-BATTELLE, LLC
for the
US DEPARTMENT OF ENERGY
Office of Nuclear Energy
under contract DE-AC05-00OR22725

CONTENTS

LIST OF FIGURES

LIST OF TABLES

ACRONYMS

ABSI-LW	auxiliary beam stress improved laser welding
appm	atomic parts per million
DIC	digital image correlation
DOE	Department of Energy
EDM	electrical discharge machining
EPRI	Electric Power Research Institute
FSW	friction stir welding
HAZ	heat-affected zone
HeIC	helium induced cracking
LTO	Long-Term Operation
LW	laser weld
LWRS	Light Water Reactor Sustainability
NE	Office of Nuclear Energy
ORNL	Oak Ridge National Laboratory
SEM/EDS	scanning electron microscopy/energy-dispersive X-ray spectroscopy
THDS	thermal helium desorption spectroscopy
VAR	vacuum arc remelting
VTI	Vacuum Technology Incorporated
wppm	weight parts per million

ACKNOWLEDGMENT

This research was sponsored by the US Department of Energy (DOE), Office of Nuclear Energy (NE), Light Water Reactor Sustainability Program, Materials Research Pathway under contract No. DE-AC05-00OR22725 with Oak Ridge National Laboratory (ORNL), managed and operated by UT-Battelle, LLC.

The authors gratefully acknowledge the program support of Xiang (Frank) Chen, Materials Research Pathway Lead of the Light Water Reactor Sustainability Program at ORNL; engineering support of Kurt Smith and Bob Sitterson; hot cell facilities and operation contributions of Mark Delph, Clay Morris, Jerid Metcalf, Tony Davis, Kevin Delabar, Rick Bowman, Scott Thurman, Scott White, Donald Caverly, and Allen Smith; characterization efforts of Travis Dixon and Stephanie Curlin.

ABSTRACT

This report describes the research activities on post-weld evaluation and characterization of the quality and properties of welds made on the first phase of repair welding campaign on irradiated Ni alloy 182. The equipment and capabilities of the campaign were developed jointly by the U.S. Department of Energy, Office of Nuclear Energy, Light Water Reactor Sustainability Program, the Electric Power Research Institute, Long Term Operations Program (and the Welding and Repair Technology Center), and Oak Ridge National Laboratory. Irradiated nickel alloy 182 with doped boron ranging from 5 wppm to 15 wppm, were laser welded in the hot cell. The weld samples were cross-sectioned and characterized. The significant, on-going effort to weld irradiated alloys with high helium concentrations and comprehensively analyze the results will eventually yield validated repair techniques and guidelines for use by the nuclear industry in extending the operational lifetimes of nuclear power plants.

This report fulfills the FY 2023 milestone M3LW-23OR0406015, “Complete the first phase of the comprehensive characterization of repair welding performed on irradiated Ni alloy 182”.

1. INTRODUCTION

Today, welding is widely used for repair, maintenance, and upgrades of nuclear reactor components. As a critical technology to extend the service life of nuclear power plants beyond 60 years, weld technology must be further developed to meet new challenges associated with the aging of the plants, such as control and mitigation of the detrimental effects of weld residual stresses and repair of highly irradiated materials. To meet this goal, a fundamental understanding of welding effects is necessary for the development of new and improved welding technologies.

Welding repair of irradiated nuclear reactor materials (such as austenitic stainless steels used for the reactor internals) is very challenging because the existence of helium in the steel, even at very low levels (*i.e.,* parts per million), can cause cracking during repair welding. Helium is a product of the boron and nickel transmutation process under intense neutron irradiation. Under the influence of high temperatures and high tensile stresses during welding, rapid formation and growth of helium bubbles can occur at grain boundaries, resulting in intergranular cracking in the heat-affected zone (HAZ) – the so-called helium-induced cracking (HeIC) (Kanne Jr. 1988). Over the past decades, a basic understanding has been established for the detrimental effects of weld stresses on HeIC (Feng and Wilkowski 2002) (Feng, Wolfe, *et al*. 2009). However, practical methods for weld repair of irradiated materials are still evolving. Industry's experience is based on current arc-welding–based and laser-welding–based repair technologies that are limited to situations where the helium in the irradiated materials is less than 10 appm. Although no welding restrictions are required for helium levels below 0.1 appm helium, restrictions on welding parameters, such as welding heat input, are necessary when the helium levels are above 0.1 appm. Reactor internals with helium levels above 5-10 appm are generally considered to be not weldable (or weld repairable) using today's welding practices common to the industry (EPRI 2015) (JNES 2004).

As the service life of nuclear reactors in the United States is extended, the amount of helium in the structural materials in certain highly irradiated areas will continue to increase, reaching levels much higher than 10 appm, as shown in **Figure 1** (EPRI 2015). Therefore, innovations in repair welding technology are essential to addressing this critical industry need.

This research, a joint effort of the US Department of Energy Office of Nuclear Energy (DOE NE) Light Water Reactor Sustainability (LWRS) Program and the Electric Power Research Institute (EPRI) Long-Term Operations (LTO) Program, is aimed at developing advanced welding technology for reactor repair and upgrades. It focuses on repair welding of irradiated materials that are extremely challenging and require long-term R&D. Multiple weld campaigns have been completed on irradiated 304 and 316 stainless steels with the targeted helium concentration up to 30 appm between FY2018 and FY2021. Microstructural characterizations demonstrated the feasibility to use advanced auxiliary beam stress improved laser welding (ABSI-LW) and friction stir welding (FSW) to mitigate the formation of HeIC. In this most recent weld campaign, irradiated nickel alloy 182 samples with targeted helium concentrations up to 20 appm were selected for ABSI-LW studies. This milestone report summarizes characterization results of the repair welding performed on these alloy 182 samples.

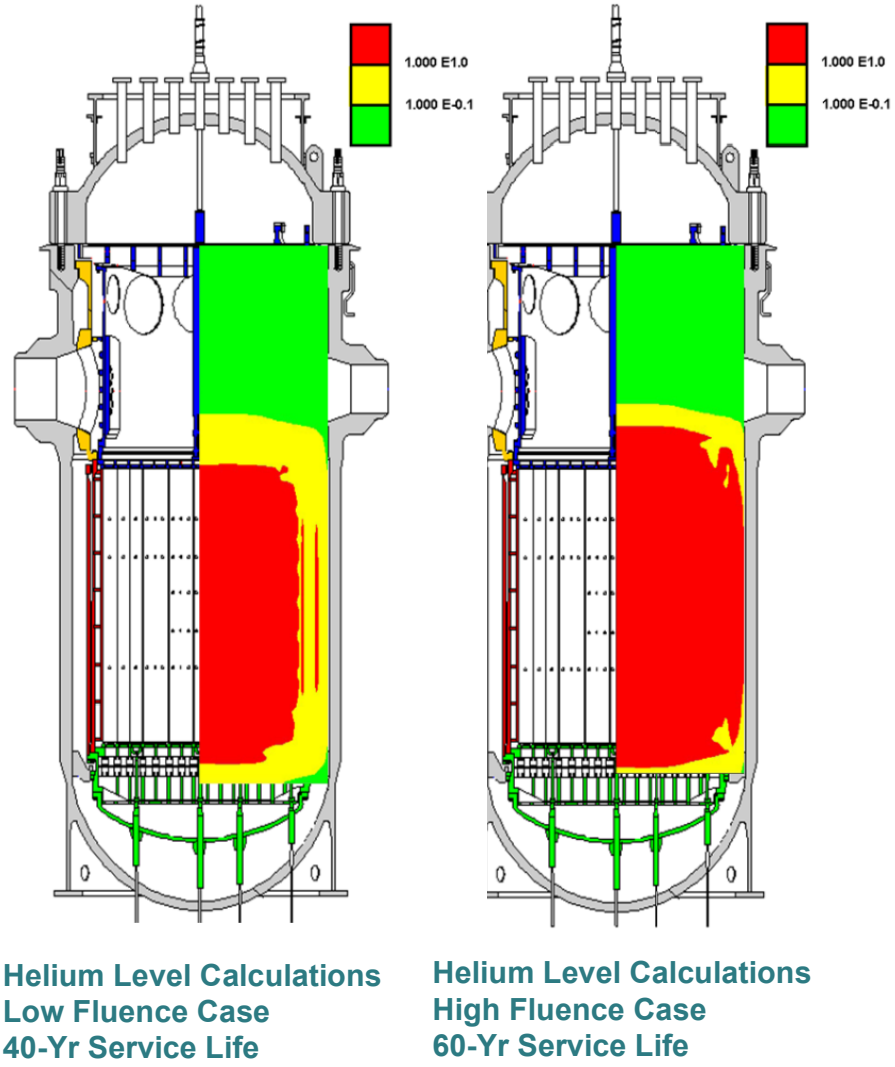

Figure 1 Forecast of helium generation of a typical Combustion Engineering (CE) pressurized water reactor. Red zone: helium generation greater than 10 appm (not weldable with current welding processes). Yellow zone: helium generation greater than 0.1 appm and less than 10 appm (weldable with heat input control). Green zone: helium generation less than 0.1 appm (no special process control is needed). From (EPRI 2015).

2. EXPERIMENTS

2.1 Materials

Five heats of Alloy 182 having five boron concentration levels (nominally 0, 5, 10, 20, and 30 ppm by weight) were produced by Sophisticated Alloys, Inc, following the specifications established by ORNL to cover the anticipated range of helium levels in materials exposed up to 80 years of reactor operation (M3LW-14OR0406014, 2014). Table **1** shows the complete chemistry analysis of the Alloys 182 heats used in this project. As shown in the Table 1, not all the target boron concentrations were achieved but a wide range of boron levels were produced ranging from 0.3 to 23 ppm. All other elements met the chemistry requirements for Alloy 182. Bar stock sections were machined to final dimensions (76x56x8.9mm^3 nominal) to yield 7 pieces at each boron level for subsequent irradiation. Alloy 182, being weld filler metal, typically has a coarser weld microstructure in reactor structures. An additional fifteen specimens from heats 182D and 182E respectively were fusion welded on one side to half of the specimen depth to produce a representative weld microstructure.

The custom alloy 182 blocks were irradiated at the ORNL High Flux Isotope Reactor with a total fluence ranging from 5.08×10^{20} to 1.31×10^{21} n/cm^2 (thermal neutrons < 0.5 eV, epithermal neutrons 0.5 eV to 0.1 MeV and fast neutrons > 1 MeV) depending on the location of the blocks inside the irradiation bores. The irradiated blocks were stored for more than 2 years to allow decay of short half-life isotopes before welding experiments began. Details of the irradiation of the coupons can be found in the previous milestone report M3LW-17OR0406013 (Feng, Miller, *et al*. 2017).

Table 1 Chemistry Analysis Results of Alloy 182

		Alloy 182 Heat Identification				
Element	Unit	182A	182B	182C	182D	182E
B	ppm	0.3	5	15	14	23
Co	ppm	2	2	2	2	2
Al	ppm	81	34	32	54	56
Mo	ppm	1	1	8	1	1
Cu	ppm	2	1	2	1	1
C	wt%	0.03	0.08	0.03	0.04	0.04
Mn	wt%	7.03	7.00	6.76	7.17	7.08
Si	wt%	0.50	0.50	0.51	0.50	0.49
Cr	wt%	15.99	16.00	16.00	16.16	16.10
Fe	wt%	7.36	7.92	7.31	7.14	7.12
Nb	wt%	2.07	2.06	1.83	1.82	1.84
Ti	wt%	0.44	0.43	0.43	0.43	0.46
P	wt%	0.00013	0.00011	0.00018	0.00015	0.00016
S	wt%	0.00207	0.00199	0.00280	0.00200	0.00220
Ni		Balance	Balance	Balance	Balance	Balance

2.2 Welding

In the most recent weld campaign, laser welding experiments were conducted on three alloy 182 coupons with three boron concentrations ranging from 5 wppm to 15 wppm). The weld coupon ID and boron concentrations are given in **Table 2.** For weld coupon 182D-W-1, the letter "W" in the ID indicates that this coupon has been fusion welded to produce a representative weld microstructure before irradiation. Both ABSI-LWs and conventional LWs without ABSI were conducted at the dedicated welding hot cell at the ORNL REDC. Details of the equipment and experimental procedures have been reported in the previous milestone report (M2LW-17OR0406014) (Feng, Miller, *et al*. 2017).

Table 2 Weld Coupon ID and their microstructural condition as well as the target and actual B concentrations

Weld Coupon ID	Microstructural condition	Target Boron, wppm	Measured boron, wppm
182B-2	Wrought	5	5
182C-1	Wrought	10	15
182D-W-1	Weld	20	14

Laser weld cladding has been performed on irradiated alloy 182 base material with 82 as the filler material. Four laser-welded clads (weld IDs L1, L2, L3 and L4) were made using different welding conditions on each coupon. The arrangement of the four laser clads on each coupon is illustrated in Figure 2. In this figure, the two three-layer claddings on the top side of the steel coupon plate are labeled as L1 and L2, and two claddings on the bottom side are labeled as L3 and L4. Weld claddings L2 and L4 in the figure were made with the ABSI-LW and weld claddings L1 and L3 were made with LW without ABSI for comparison. Each weld clad consisted of three layers (Layer 1, layer 2 and Layer 3 from the bottom to the top of each clad). Layer 1 consisted of ten or eleven weld passes. Layer 2 consisted of seven or eight weld passes. Layer 3 consisted of four weld passes. The welding sequence of each layer is denoted using the numerical numbers as shown in **Figure 2.** In addition, single-pass welding (labeled as SL or SH) was also conducted. The purpose is to validate the effective heat input after the weld samples are cut. The relative locations of the single-pass welds are indicated in **Figure 2**. The welding direction of all weld passes was consistently towards the positive direction of the X axis. The Y-coordinates of the first and the last weld passes in Layer 1, as well as the Y- coordinates of the single pass welds, were also shown in **Figure 2**.

Note 1: For coupon 182D-W-1, single-pass SL and multi-pass L1 and L2 were cladded on the weld structure side that was produced by autogenous fusion welding on one side of the coupon to represent weld microstructures prior to irradiation.

Note 2Some weld passes in **Figure 2** are marked by a superscript '*'. This indicates abnormal welding parameters or conditions was accidentally used in these weld passes. Details will be described in the subsequent sections.

Note 3: A new wire feeder was installed before this weld campaign and the new wire feeder was not perfectly aligned with X-axis as it should be **(Figure 3**). To compensate this change, the sequence of weld passes was adjusted as "from right to left" (towards the negative direction of Y-axis) except for the first layer of L1 and L3 on 182B-2. In the previous campaign, the sequence of laser welding passes was always "from left to right" (towards the positive direction of Y-axis).

182B-2

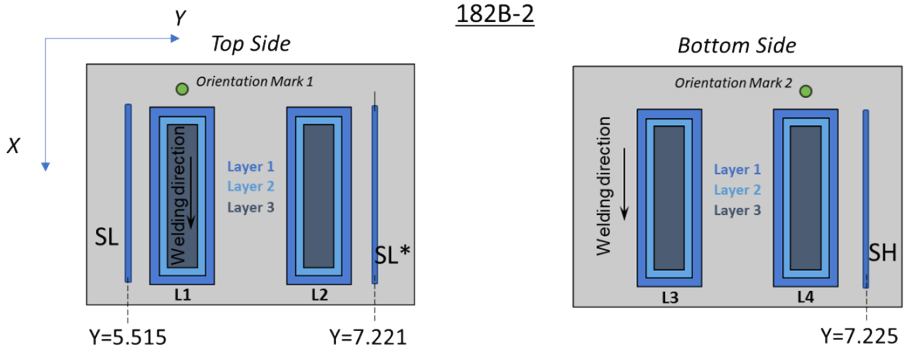
Y
X
Top Side
Orientation Mark 1
Welding direction
Layer 1
Layer 2
Layer 3
SL
SL*
L1
L2
Y=5.515
Y=7.221
Bottom Side
Orientation Mark 2
Welding direction
Layer 1
Layer 2
Layer 3
SH
L3
L4
Y=7.225

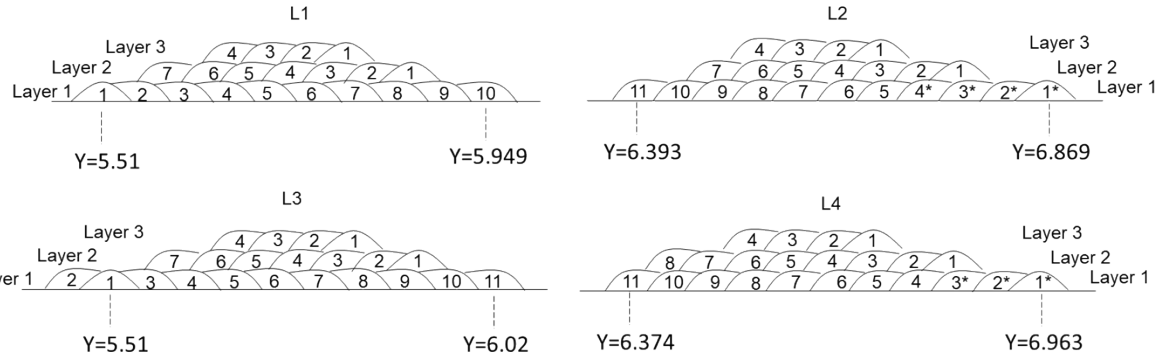
L1
Layer 3
Layer 2
Layer 1
Y=5.51
Y=5.949
L2
Layer 3
Layer 2
Layer 1
Y=6.393
Y=6.869
L3
Layer 3
Layer 2
Layer 1
Y=5.51
Y=6.02
L4
Layer 3
Layer 2
Layer 1
Y=6.374
Y=6.963

182C-1

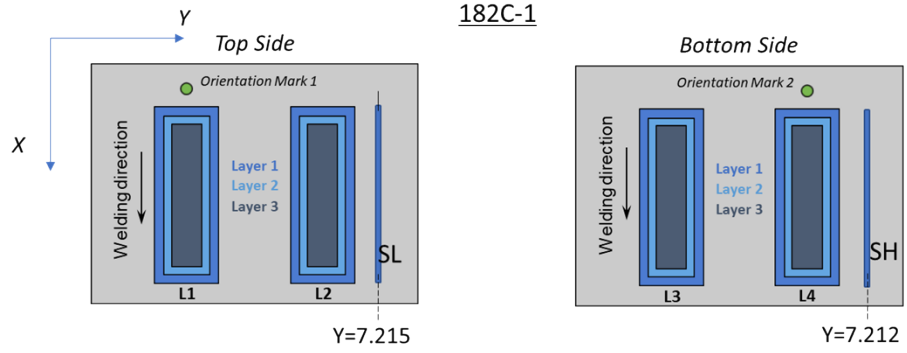
Y
X
Top Side
Orientation Mark 1
Welding direction
Layer 1
Layer 2
Layer 3
SL
L1
L2
Y=7.215
Bottom Side
Orientation Mark 2
Welding direction
Layer 1
Layer 2
Layer 3
SH
L3
L4
Y=7.212

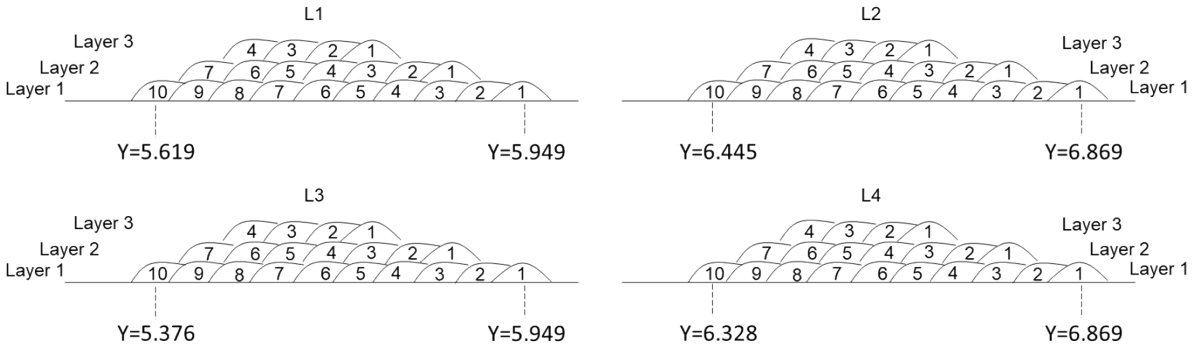
L1
Layer 3
Layer 2
Layer 1
Y=5.619
Y=5.949
L2
Layer 3
Layer 2
Layer 1
Y=6.445
Y=6.869
L3
Layer 3
Layer 2
Layer 1
Y=5.376
Y=5.949
L4
Layer 3
Layer 2
Layer 1
Y=6.328
Y=6.869

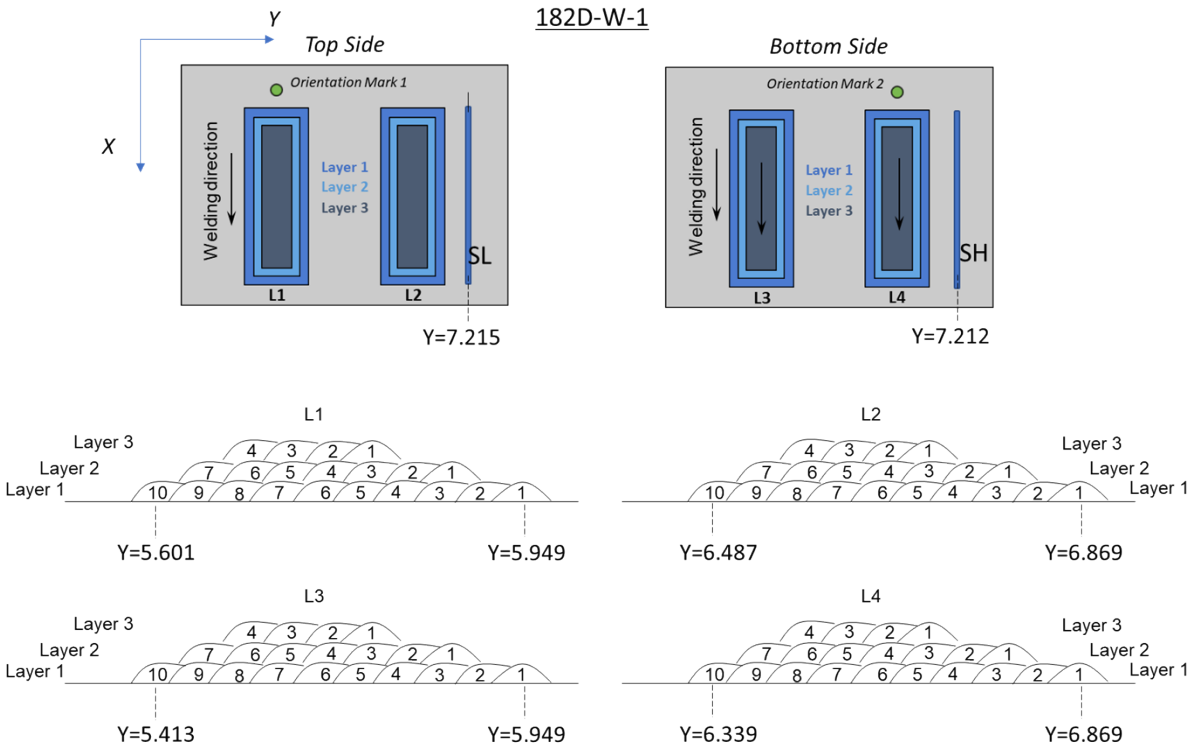

Figure 2 Weld Layout for LW of Irradiated Coupons. Superscript * indicates abnormal welding parameters or conditions (unit of the location at Y: mm).

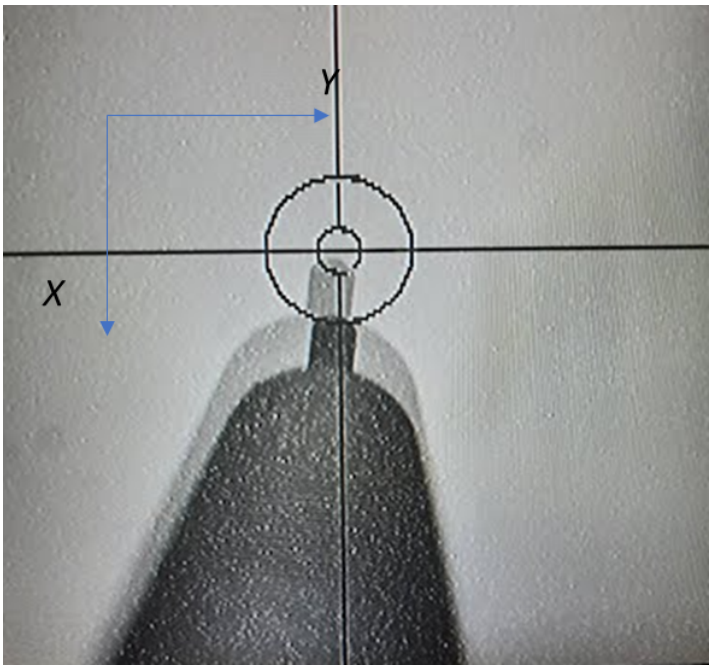

Figure 3 Image of the new wire feeder showing a tilted angle with respect to the welding direction (positive direction along X-axis). The ghost reflection is due to the optical filters and lenses in the collimated camera system.

The essential laser weld cladding parameters are given in **Table 3.** Typically, within each completed cladding, identical welding parameters were applied. Weld clads L1 and L2 had a higher laser cladding speed and low heat input than weld clads L3 and L4 in these experiments. Therefore, each weld coupon had four weld claddings (L1 through L4) performed with four different welding conditions. Additional single-pass LW passes without ABSI, labeled as SL and SH in **Figure 2,** were performed to evaluate the effect of heat input and weld bead profile of a single LW pass on HeIC. The letter "S" in the label stands for single-pass weld. "L" or "H" stands for low-heat or high-heat parameter set. This provides the ability to isolate the effect of multi-thermal cycles in the multi-pass, multi-layer clads. Single pass welds also allow for the determination of the base metal percentage dilution of the first weld layer by for each LW parameter set. The percentage Base Metal Dilution = 100 X (Area of Base Metal Melted /Area of Deposited Weld). Furthermore, the weld dilution may also be used to estimate what the maximum helium content of the first layer or individual weld pass could be assuming the helium does not escape the weld pool. It is expected that only a portion of the helium remains in the first weld layer or individual weld pass and successively lower amounts as more layers are applied. Removing specimens for helium measurement to determine the percentage helium remaining also provides an estimate of how many layers are required before conventional welding methods may be used to complete the reactor repair or modification. The welding condition for SL was identical to that in L1; The welding condition for SH was identical to that of L3. The different welding speeds and corresponding wire feed rates resulted in different individual weld and clad layer thicknesses.

Note, abnormal welding parameters or conditions were accidentally used in some of the passes. They mostly occurred when welding coupon 182B-2. These abnormal conditions include:

(a) The first attempt of single pass (labeled as SL* at the top side of Y-coordinate 7.221) on 182B-2 was conducted using an incorrect wire feed speed of 13.1inch/min. It should be 50 inch/min. Therefore, another single pass was conducted using the right wire feed speed (labeled as SL at the top side of Y-coordinate 5.515).

(b) For weld passes 1-4 in Layer 1 of clad L2 on 182B-2, the welds were not sufficiently protected by the shielding gas due to improper position of the nozzle. This may result in excessive surface oxidization, increased heat absorption, and hence slightly deeper weld penetration.

(c) For weld passes 1-3 in Layer 1 of clad L4 on 182B-2, incorrect raster scanning power (2000W) was used. The correct scanning power should be 368W. It resulted in excessive melting.

Table 3 Laser Weld Cladding Parameters

Parameter	Multi-pass Weld Clads				Single-Pass Weld	
	L1	**L2**	**L3**	**L4**	**SL**	**SH**
Travel speed (in./s)	0.45 (high-speed)	0.45 (high-speed)	0.083 (low-speed)	0.083 (low-speed)	0.45 (high-speed)	0.45 (high-speed)
Expected effective heat input from welding beam (kJ/in)	0.39 (low-heat)	0.39 (low-heat)	1.20 (high-heat)	1.20 (high-heat)	0.39 (low-heat)	1.20 (high-heat)
Wire feed speed (in./min)	50	50	13.1	13.1	50	13.1
Laser welding power (W)	1,000	1,000	1,000	1,000	1,000	1,000
Laser welding diameter (mm)	2	2	2	2	2	2

ABSI	No	Yes	No	Yes	No	No
ABSI laser power (W)	N/A	2000	N/A	368	N/A	N/A
ABSI laser diameter (mm)	N/A	7.5	N/A	7.5	N/A	N/A

2.3 Post-Weld Evaluation and Characterization

A horizontal band saw was used in a hot cell to cut cross-weld samples from the welds made on irradiated coupons for weld quality, microstructure and property characterization. Samples for helium determination were removed by a low speed diamond saw in a hot cell. Details of the cutting procedures can be found in the previous milestone report M2LW-18OR0406014 (Feng, Tang, et al. 2018).

Figure 4 shows the layout of samples taken from a LW clad coupon post-weld evaluation. These post-weld evaluation samples were cut transverse to the weld travel direction. Samples labeled from 1 to 14 are located on the multi-pass LW claddings (L1, L2, L3 and L4). Samples 15 to 18 were cut from the single-pass LWs (SL and SH). Samples 1 through 7 contain LW claddings L1 and L4, and 8 through 14 contain LW claddings L2 and L3. In addition, three small samples at the bottom left corner were removed for future helium measurement. The remaining material were kept at the LAMDA facility of ORNL for future studies. For coupon 182D-W-1, single-pass SL and multi-pass L1 and L2 were cladded on the weld structure side.

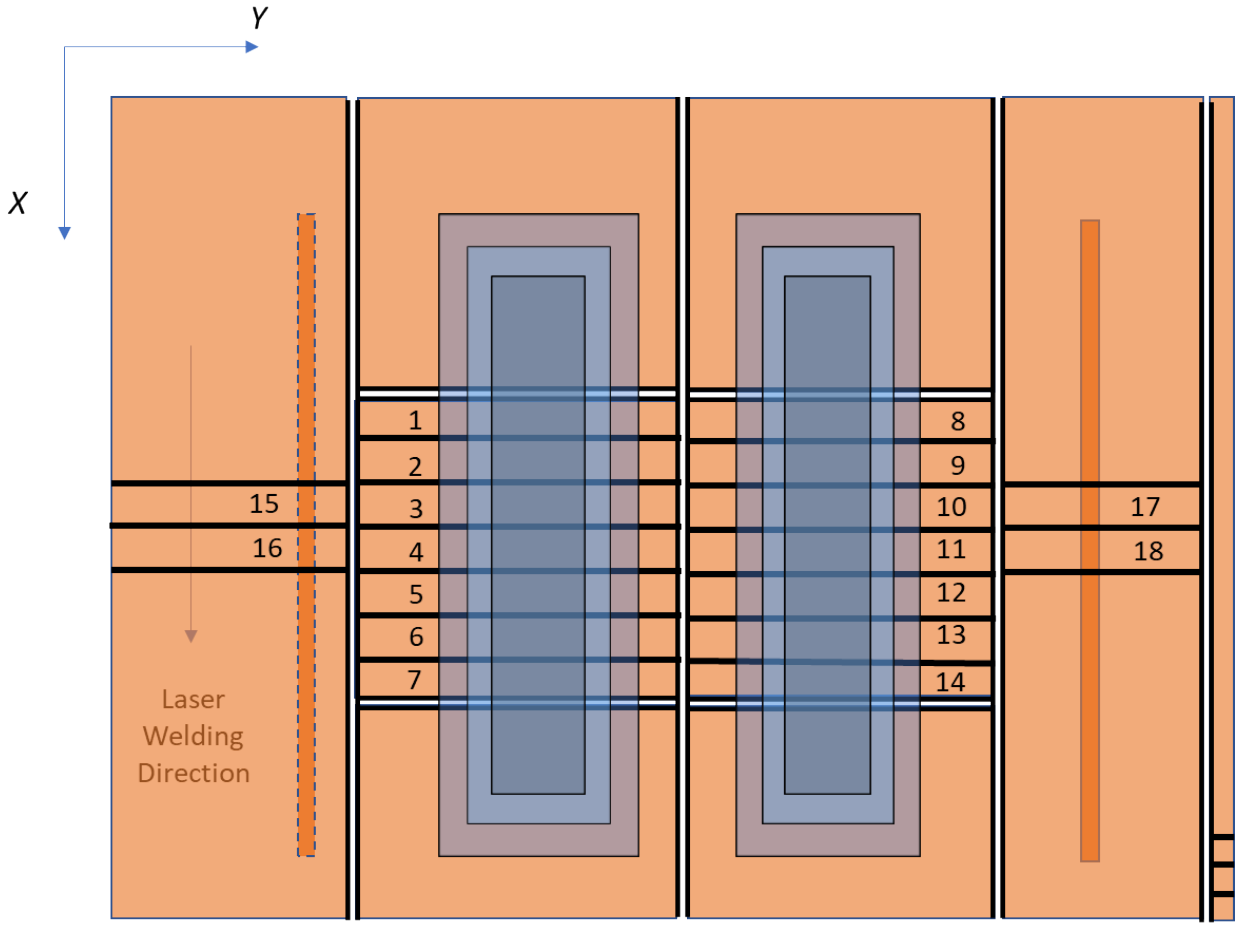

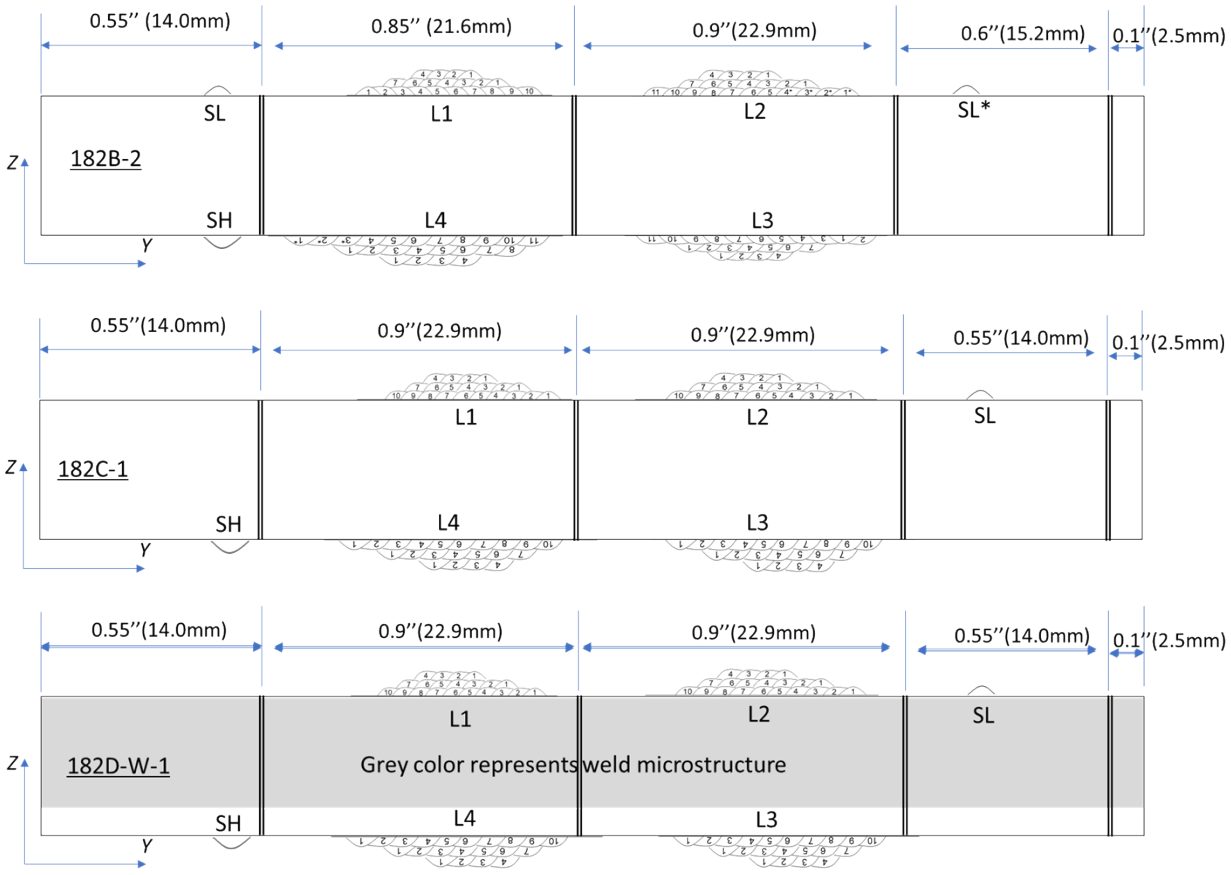

Figure 4 The drawing of the cut and the relative location of each weld pass

3. RESULTS AND DISCUSSION

Figure 5 shows the cross-sections of all single-pass welds. Overall, the fusion zone created by the low heat input parameters (labeled as SL) was smaller than that created by high heat input parameters (labeled as SH). With high heat input parameters, the tendency of HeIC increased with boron concertation. One small crack was observed on the left side of the weld toe in the coupon with 5 wppm boron (182B-2-15-SH). Although no cracks were found in the coupon with 15 wppm boron (182C-1-15-SH), larger cracks were observed on both sides of the weld toe in the coupon with 14 wppm boron (182D-W-1-16-SH). While with low heat input parameters, HeIC was not observed in coupons with 5 and 15 wppm doped boron (182B-2-15-SL and 182C-1-18-SL), but small cracks did occur at the right side of the weld toe and the bottom of the weld in the coupon with 14 wppm doped boron (182DW-1-17-SL). The possible cause might be as follows. This single-pass weld (182DW-1-17-SL) was performed on the weld microstructures that was purposely created by the fusion welding process before irradiation. During the fusion welding, boron could segregate and concentrated at grain boundaries in HAZ (Chen, 2001), leading to locally high helium concentration after irradiation. Such regions with high helium concentration were more susceptible to HeIC during the subsequent laser welding.

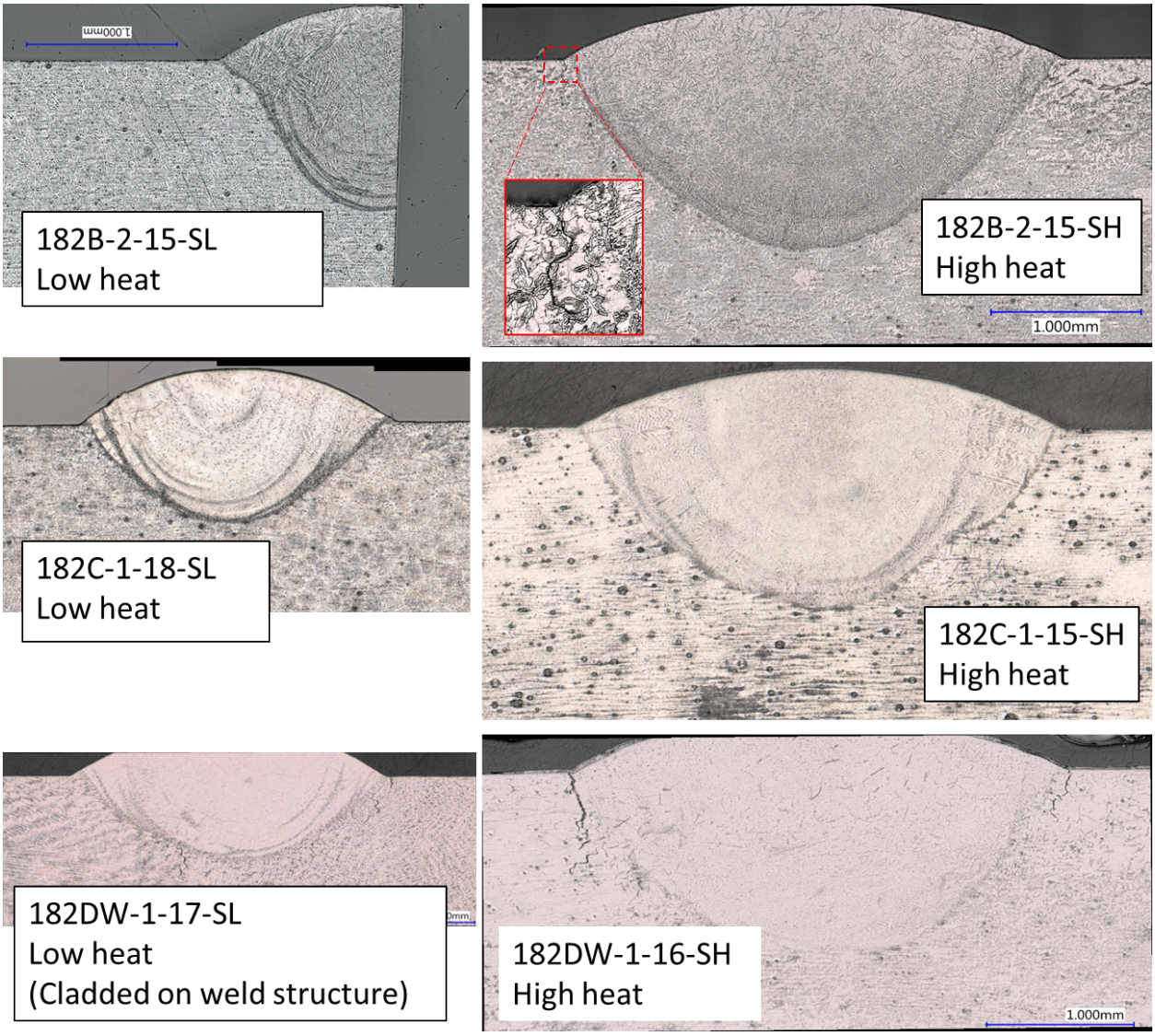

Figure 5 Cross-section views of single-pass welds.

Figure 6 shows the cross-sections of the multi-pass weld clads performed on the coupon with 5 wppm B using 4 different welding conditions as listed in **Table 3**. With the welding condition of low heat input without ABSI (**Figure 6a**), a small crack occurred on the left side of the first weld pass in the first clad layer. The detail can be seen in the high-magnification image (labeled as "1") at the corresponding location. Grain boundary degradation was observed through the rest of the HAZ (a list of images labeled from "2" to "25" in **Figure 6a**). When ABSI is incorporated, the same amount of heat input condition also yielded a small crack at the toe of the entry weld pass (**Figure 6b**). Note, this crack could also possibly be a result of the insufficient gas shielding during the laser welding operation as mentioned before (insufficient shielding gas for passes 1-4 in Layer 1 of clad L2 on 182B-2). Interestingly, the tendency of grain boundary degradation seems reduced with ABSI, which is consistent to our previous studies on the stainless steels (Chen, 2021). For the high heat input condition with and without ABSI (**Figure 6c and Figure 6d**), cracks were also observed on the entry side of the weld toe in both cases, and ABSI seems helpful to reduce the gran boundary degradation. The reason why the cracks mostly occurred at the toe of

the first weld pass is because all weld passes except the 1st pass had a 50% overlap during cladding. The base metal absorbed more heat during welding the 1st pass than the subsequent pass. When welding the subsequent passes, a portion of the heat was absorbed by the previously deposited metal. This is why the weld penetration was deeper and cracks were more likely occur on the entry side. Further investigation is required to optimize the welding condition and ABSI parameters to reduce the formation of HeIC at the weld toe and the surface cracks. It is noted that surface cracks occurred on the top of the weld clad in the low heat input condition with ABSI (**Figure 6b**), the cause might be related to solidification cracking due to the interaction of the scanning beam with the liquid pool.

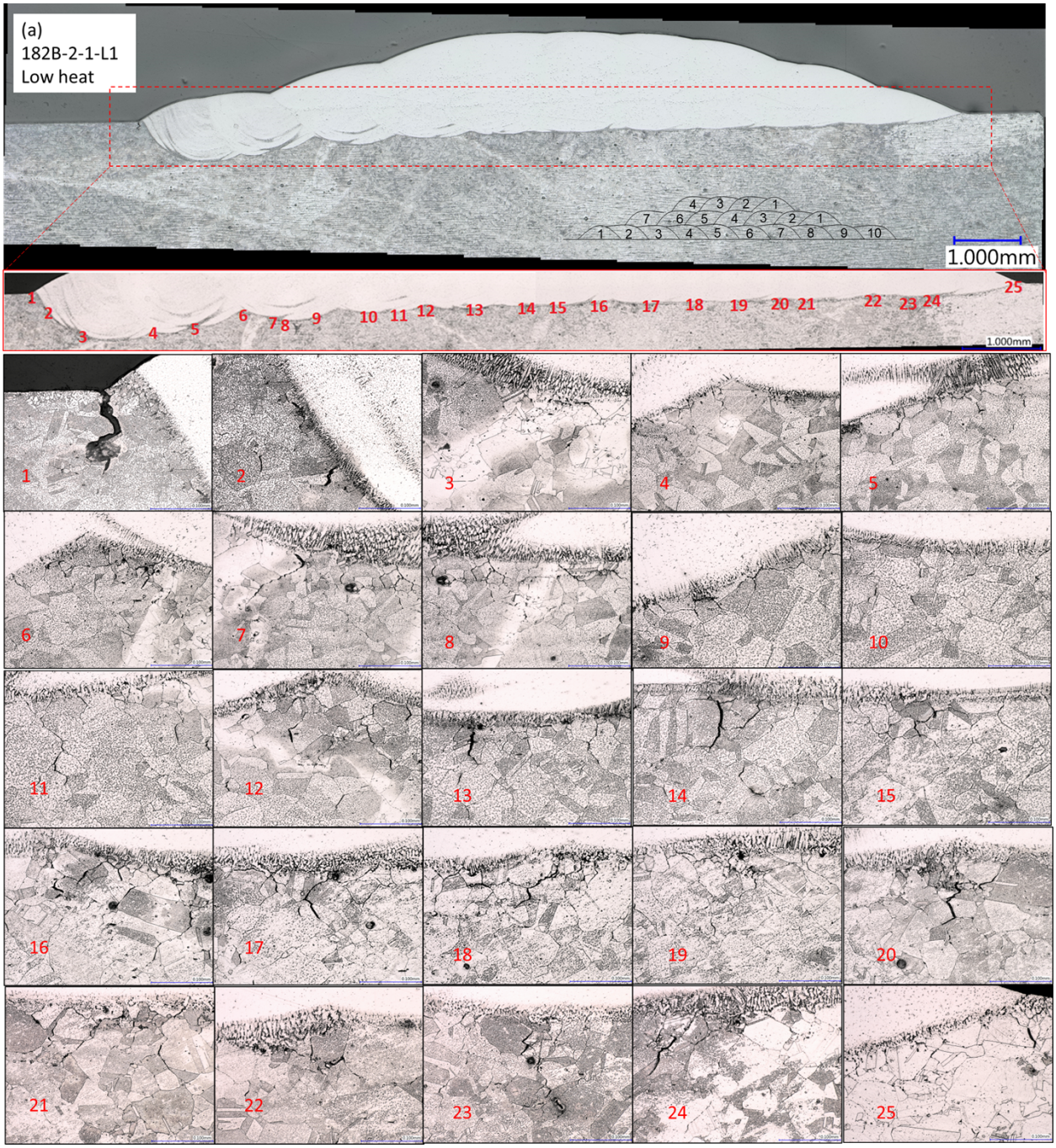

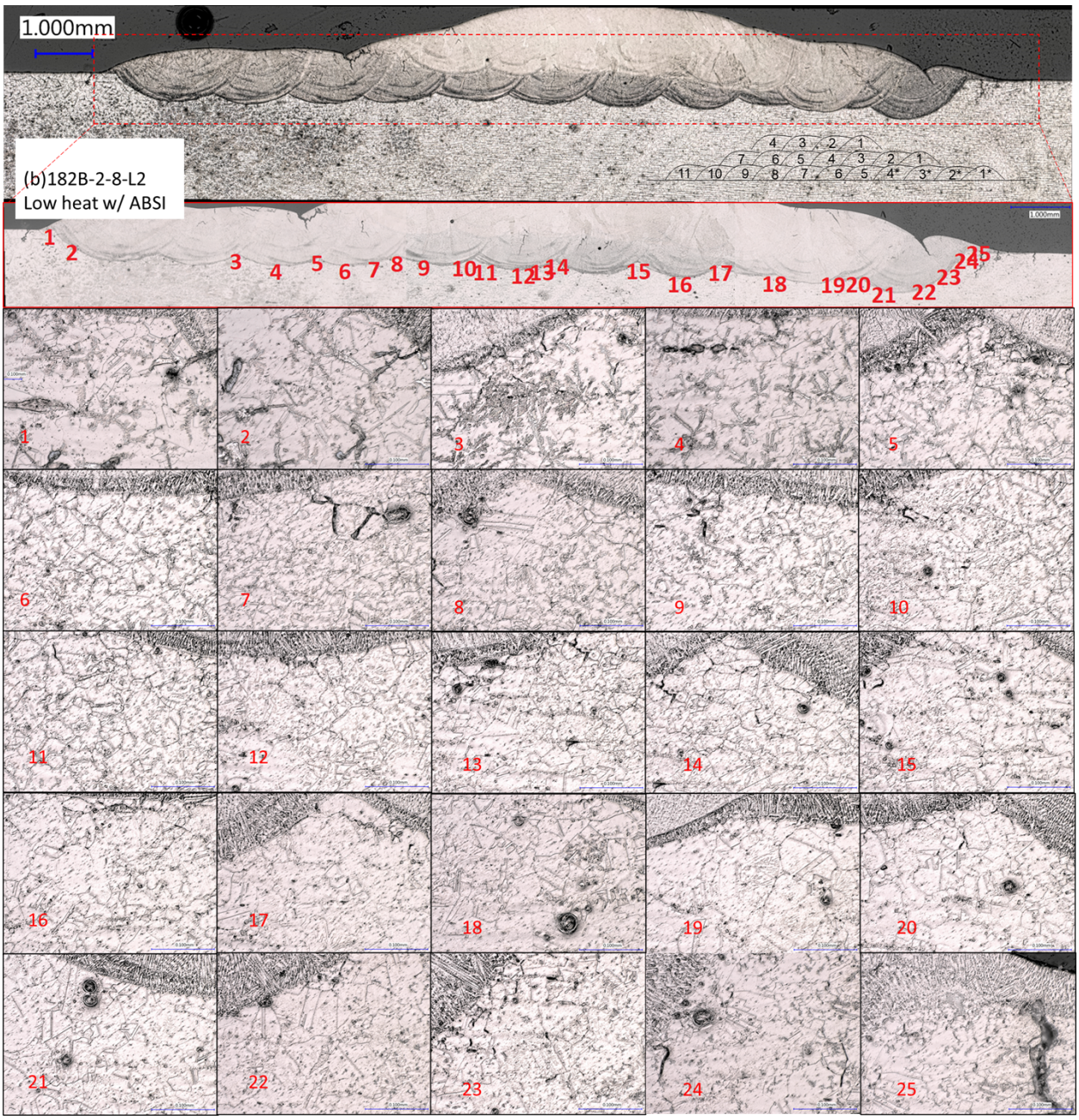
1.000mm
(b)182B-2-8-L2
Low heat w/ ABSI
1
2
3
4
5
6
7
8
9
10
11
12
13
14
15
16
17
18
19
20
21
22
23
24
25

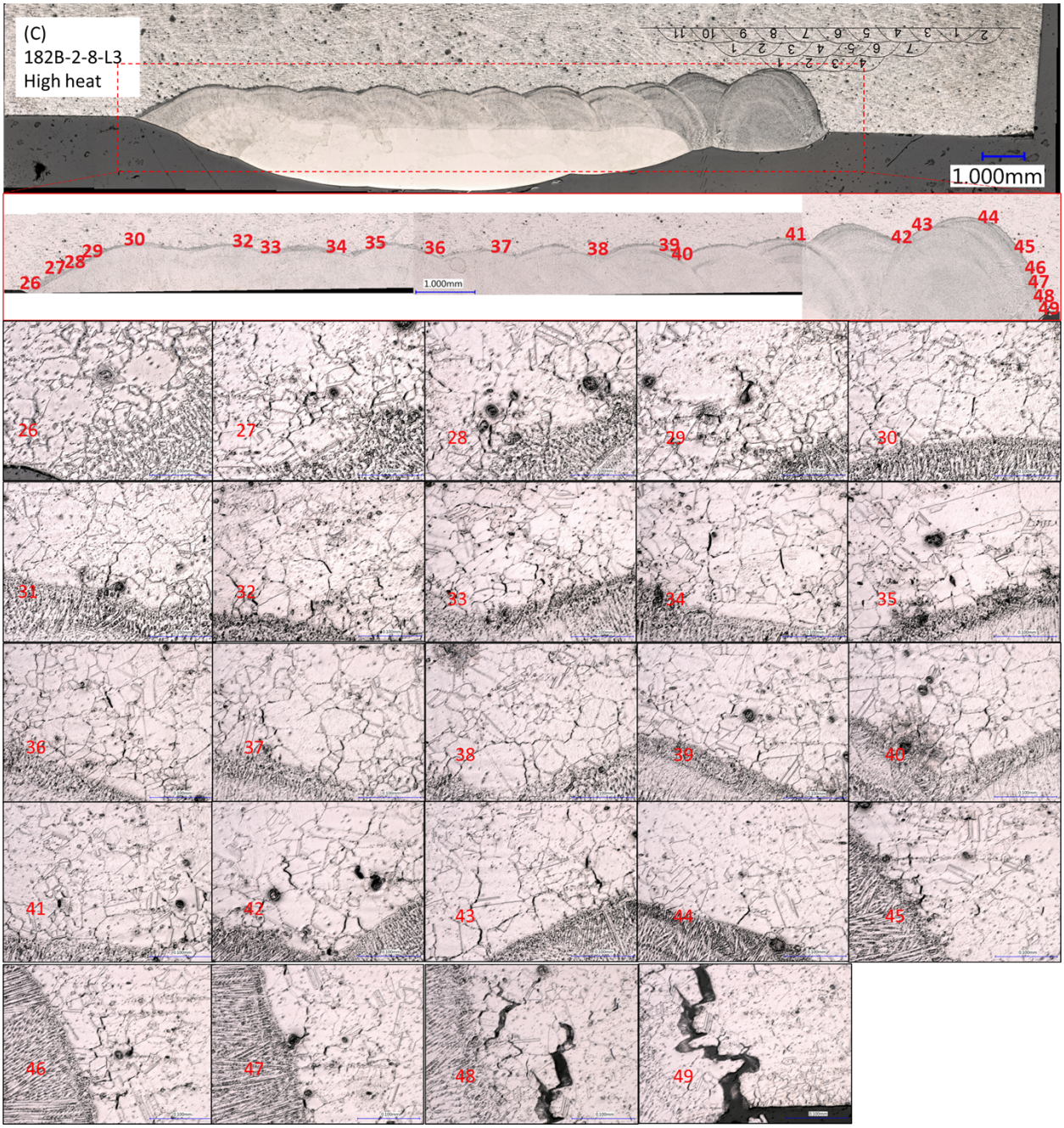
(C)
182B-2-8-L3
High heat
1.000mm
26
27
28
29
30
32
33
34
35
36
37
38
39
40
41
42
43
44
45
46
47
48
49

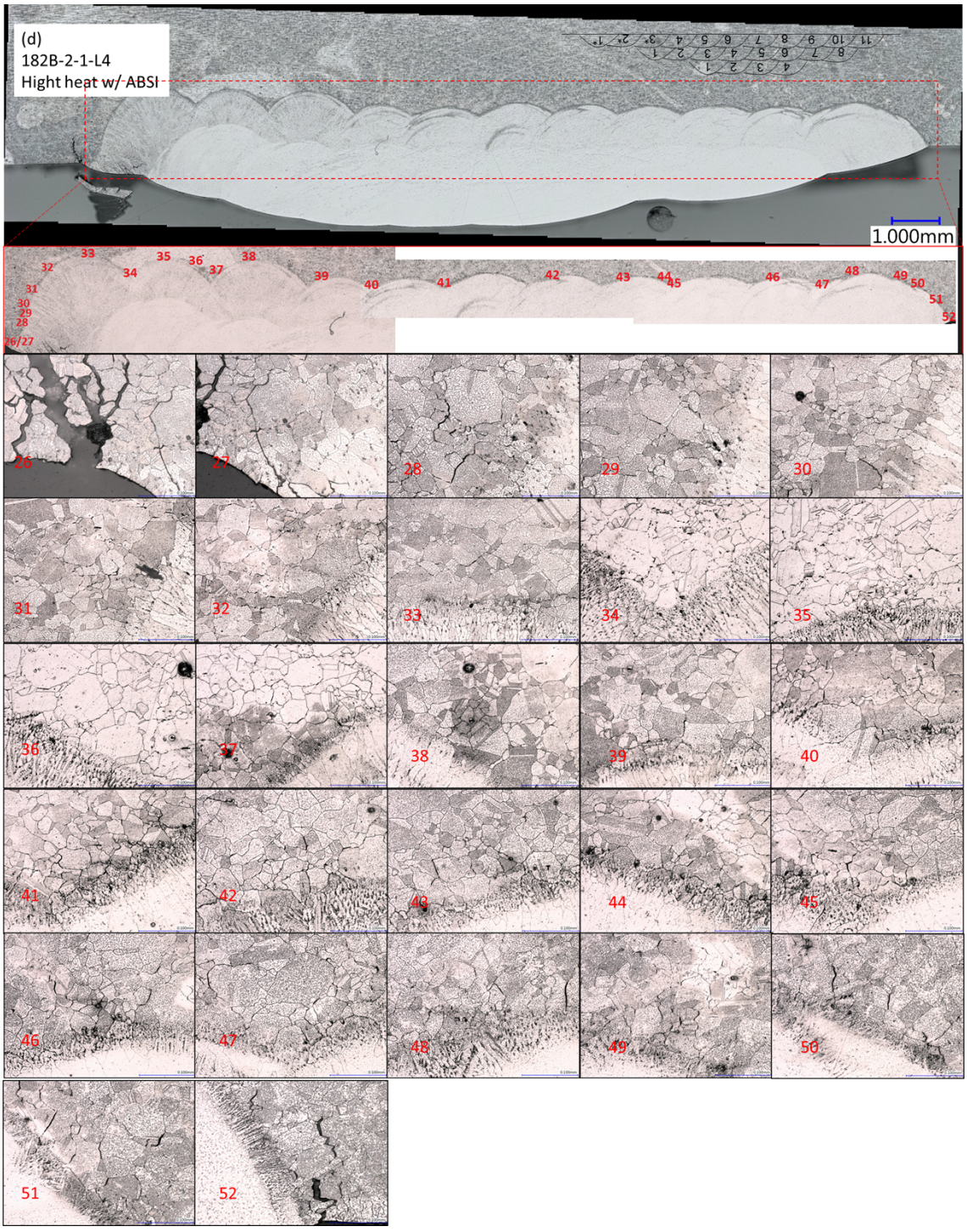

Figure 6 Cross-section views of LW cladding of alloy 182 with 5 wppm B with different welding conditions: (a) low heat input without ABSI; (b) low heat input with ABSI; (c) high heat input without ABSI; (d) high heat input with ABSI.

Figure 7 shows the cross-sections of the multi-pass weld clads performed on the coupon with 15 wppm B with different welding conditions. The results are similar to what was obtained on the coupon with 5 wppm B: (1) The entry pass had deeper penetrations and high tendency of crack formation at the weld toe; (2) ABSI was helpful to reduce grain boundary degradation; (3) surface cracks occurred in the low heat input condition with ABSI. It is worth to mention that cracks were not observed in the single-pass weld (182C-1-15-SH) but did occur at the weld to of the multi-pass sample (182C-1-8-L3) with the same welding laser parameters. The reason could be related to the repeated heat input of multi-pass welding.

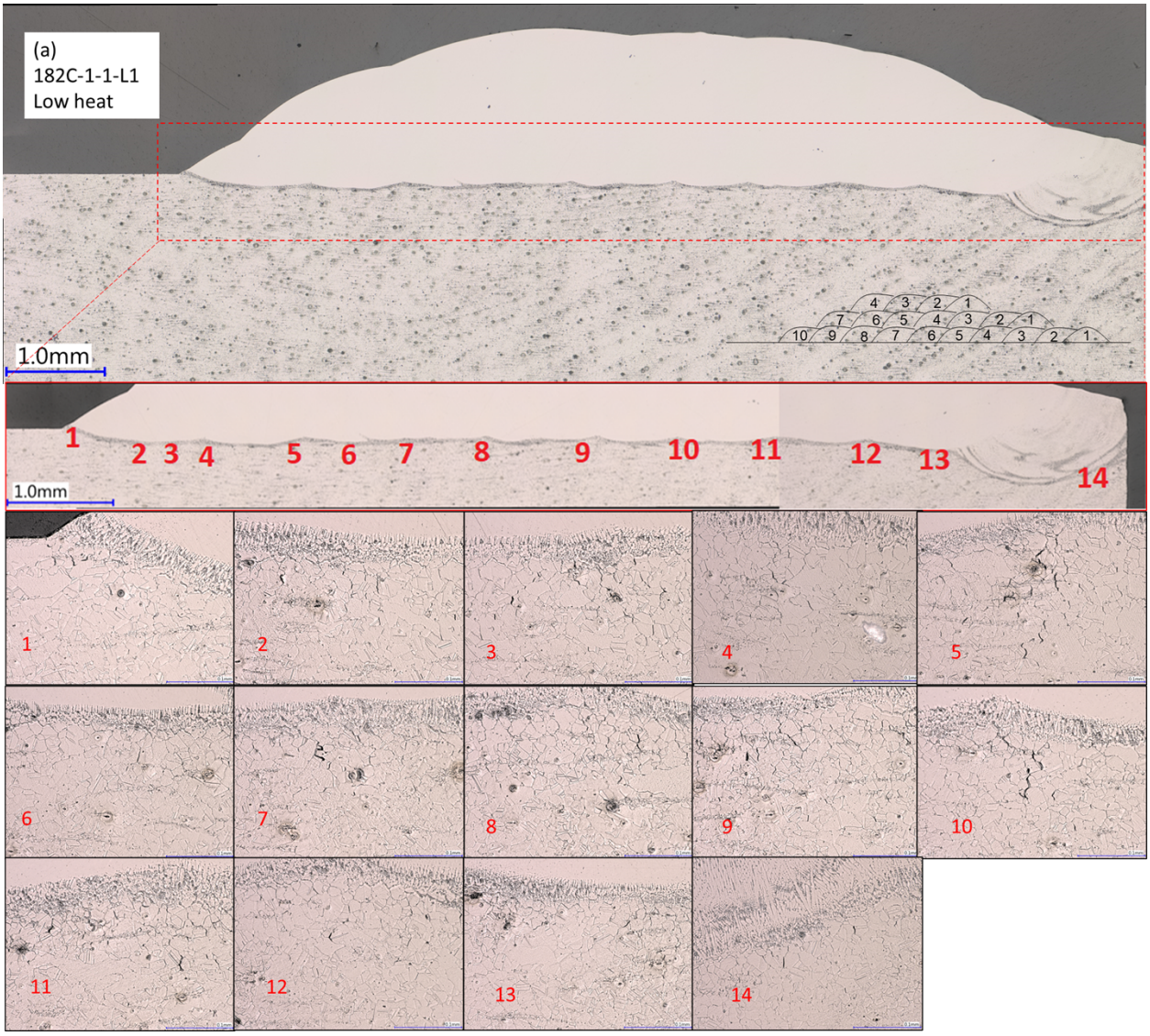

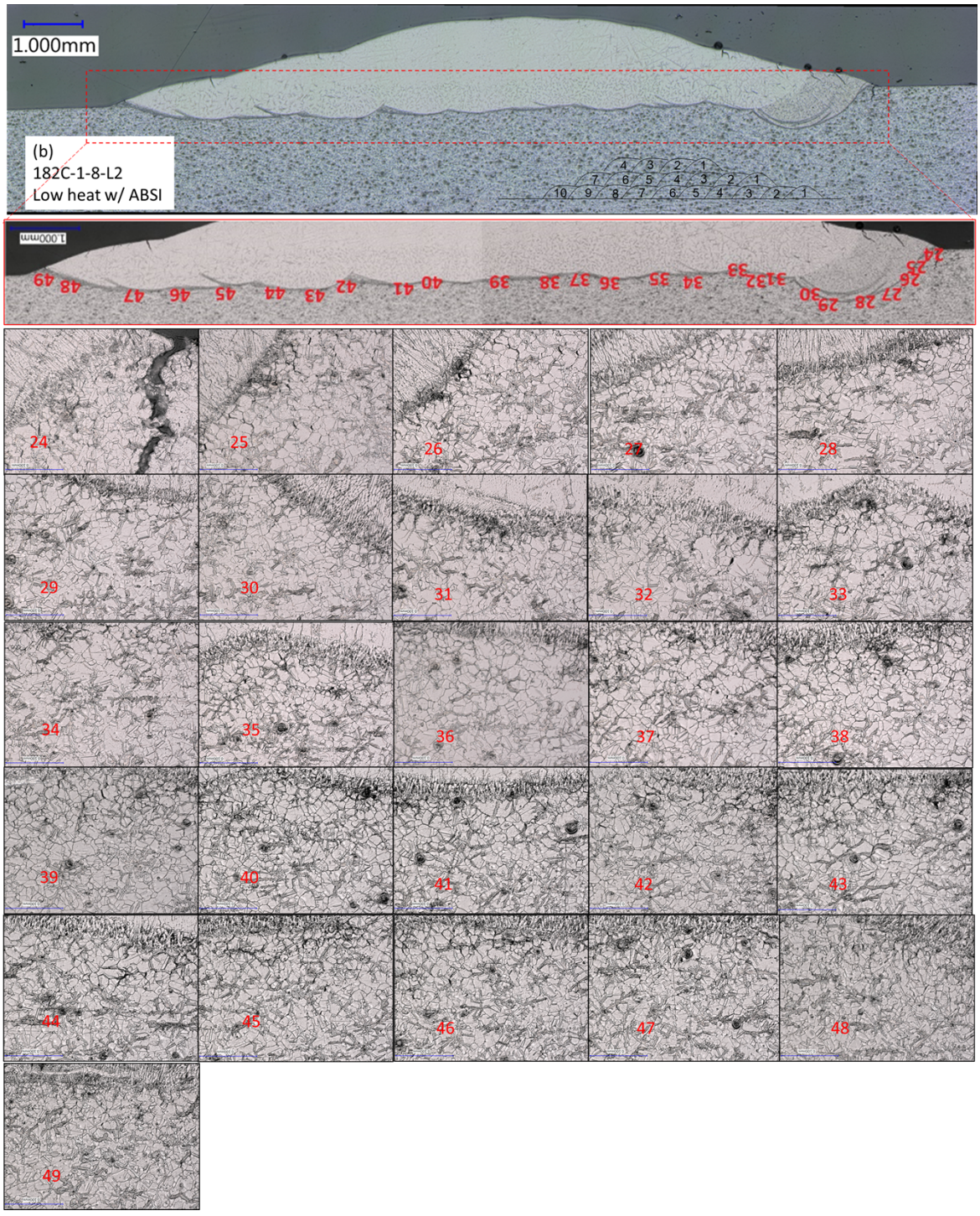
1.000mm
(b)
182C-1-8-L2
Low heat w/ ABSI
24
25
26
27
28
29
30
31
32
33
34
35
36
37
38
39
40
41
42
43
44
45
46
47
48
49

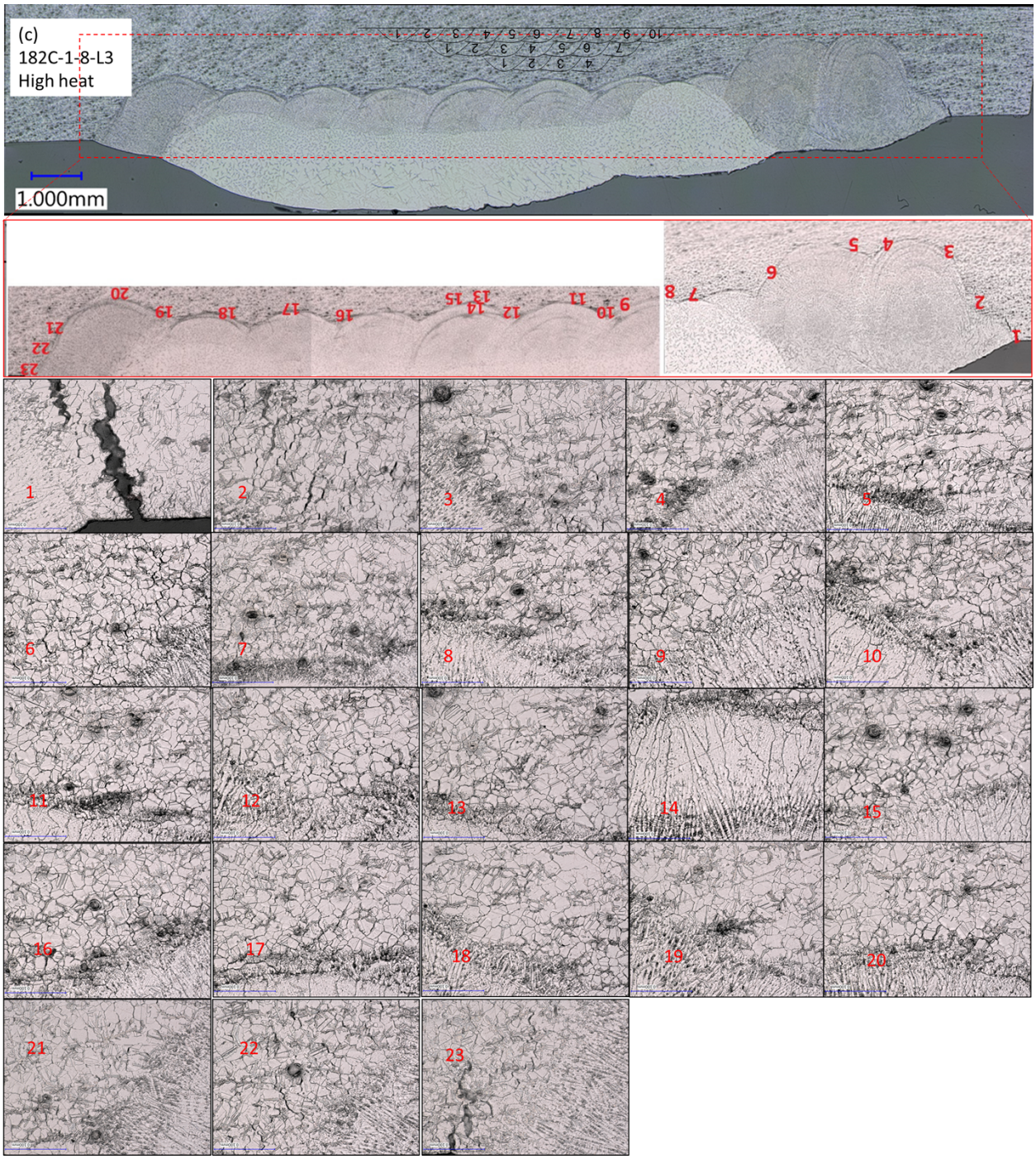
(c)
182C-1-8-L3
High heat
1.000mm

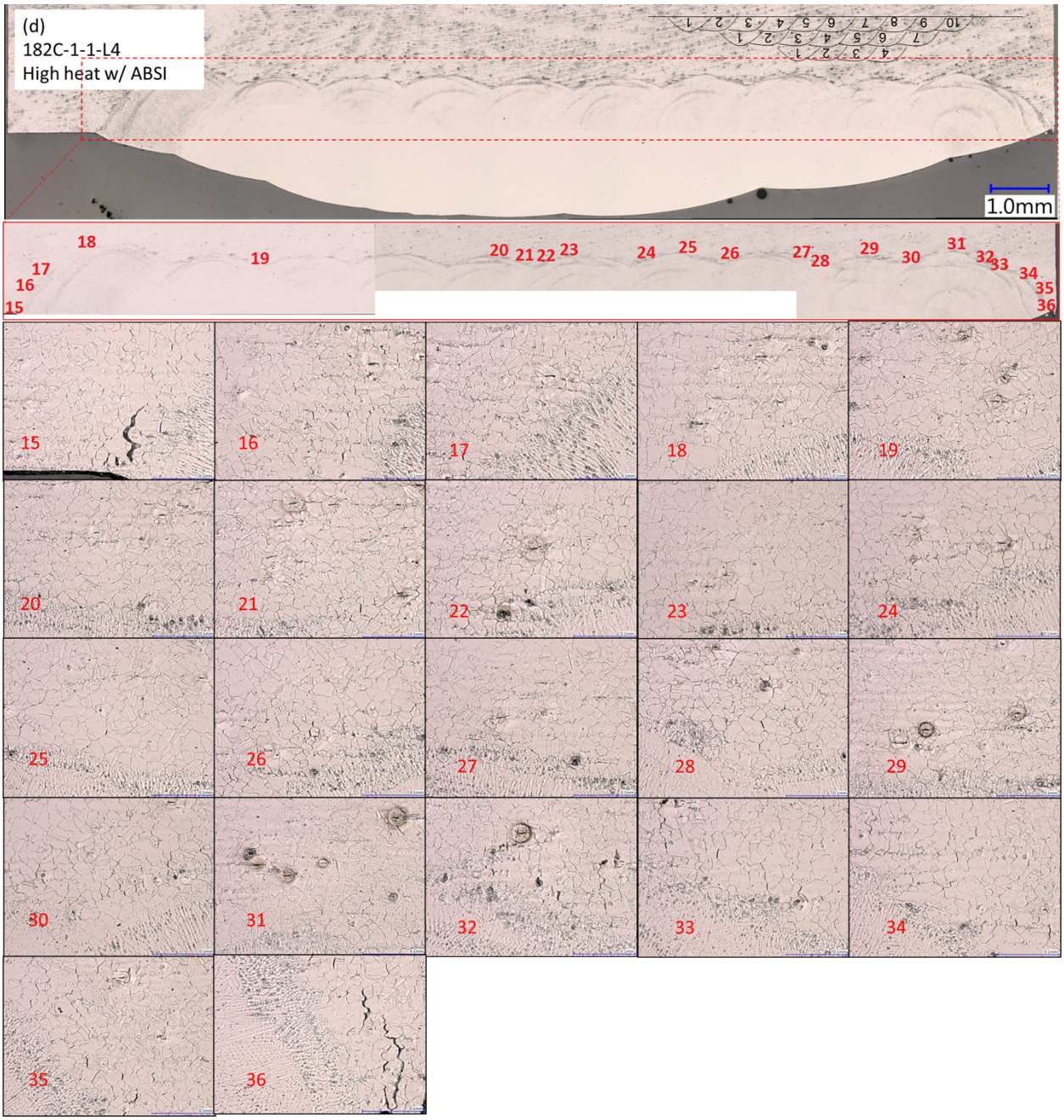

Figure 7 Cross-section views of LW cladding of alloy 182 with 15 wppm B with different welding conditions: (a) low heat input without ABSI; (b) low heat input with ABSI; (c) high heat input without ABSI; (d) high heat input with ABSI.

As mentioned previously, weld coupon 182DW had a weld microstructure produced prior to irradiation at HFIR. **Figure 8** shows the cross-section of the microstructure after laser welding. Two weld clads with low laser heat input (182DW-1-1-L1 and 182DW-1-8-L2) were performed on the weld microstructure side, and the other two clad with high laser heat input (182DW-1-1-L4 and 182DW-1-8-L3) were performed on the original base metal side.

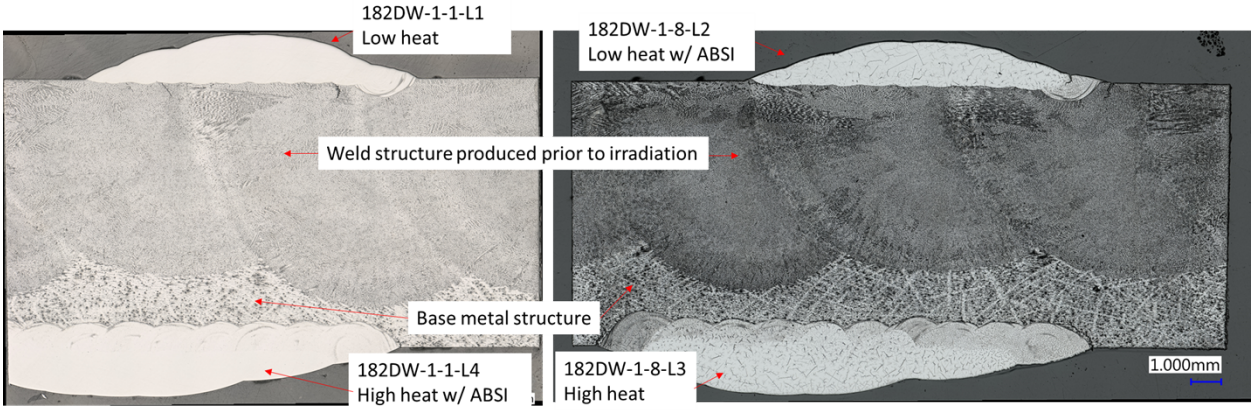

Figure 8 Cross-section views of LW cladding of alloy 182 with 14 wppm B to show the relative location of the weld microstructure produced prior to HFIR irradition.

Figure 7 shows the cross-sections of the multi-pass weld clads performed on the coupon with 14 wppm B (182DW-1) investigated in the current weld campaign with four different welding conditions. The two weld clads with high laser heat input were produced on the original base metal side consistent to other weld samples (182B-2 with 5 wppm B and 182C-1 with 15 wppm B). **Figure 7c** presents the results of high heat input condition without ABSI. Cracks were observed not only on the entry side but also the exit side of the weld toe. Slightly higher tendency of grain boundary degradation was also observed compared with sample 182C-1 with 15 wppm B. With the assistance of ABSI, amount of the grain boundary degradation seems slightly reduced as shown in **Figure 7d**. However, weld toe crack at the exit side still occurred. A portion of the weld section close to the entry pass side is missing due to bad cutting, but it is reasonable to assume that a weld toe crack also occurred at the entry pass side. Compared with 182C-1 with 15 wppm B (**Figure 7c** and **Figure 7d**), 182DW-1 with14 wppm B (**Figure 7c** and **Figure 7d**) seems to have a higher tendency of HeIC formation and grain boundary degradation. This suggest that the fusion welding performed prior to the irradiation might have an influence even on the base metal side.

In the two low heat input welds with ABSI (**Figure 9a**) and without ABSI (**Figure 9b**), a relatively large number of cracks were observed throughout the entire HAZ, compared with the high heat input welds (**Figure 9c and Figure 9d**). In general, low heat input leads to less HeIC. The discrepancy is more likely due to the influence of the weld microstructures produced prior to irradiation. As mentioned in the previous paragraphs, pre-existing weld microstructures could lead to a locally high concentration of boron due to segregation at the grain boundaries (Chen, 2001), and hence high localized He concentration after transmutation through irradiation. During laser welding, the local high concentration of He could induce a significant amount of HeIC even with relatively low heat input.

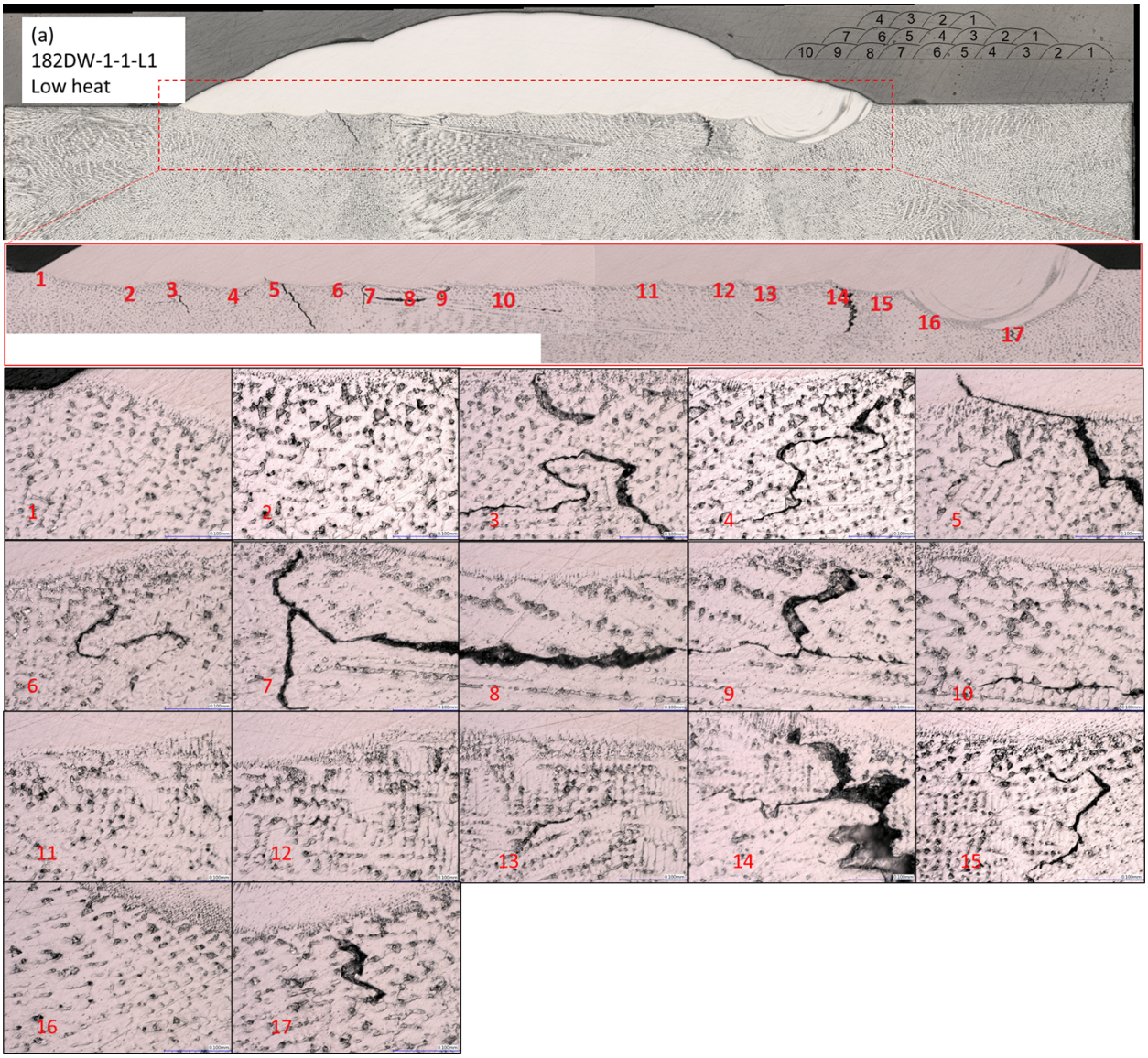
(a)
182DW-1-1-L1
Low heat
1
2
3
4
5
6
7
8
9
10
11
12
13
14
15
16
17

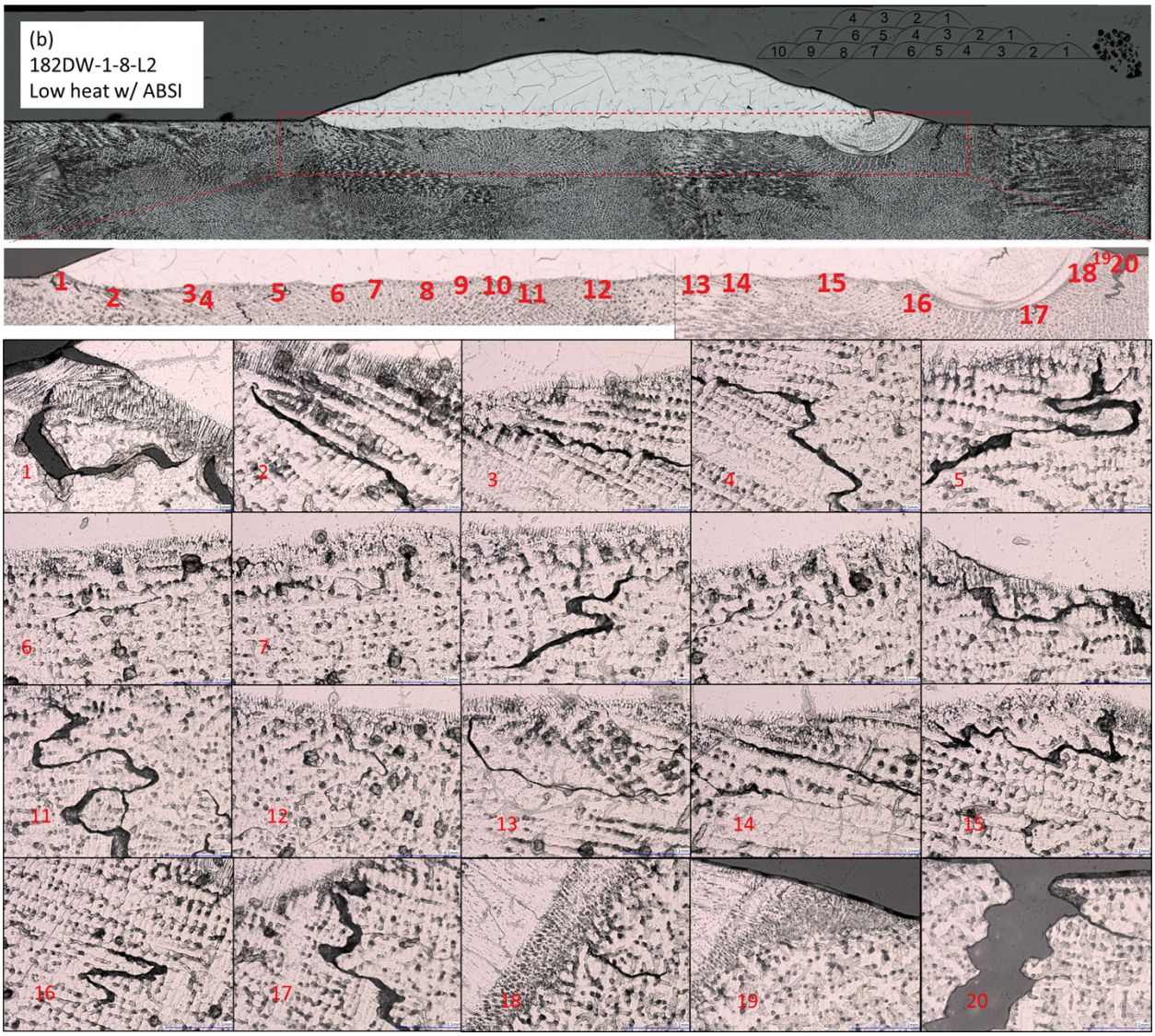
(b)
182DW-1-8-L2
Low heat w/ ABSI
1 2 3 4 5 6 7 8 9 10 11 12 13 14 15 16 17 18 19 20

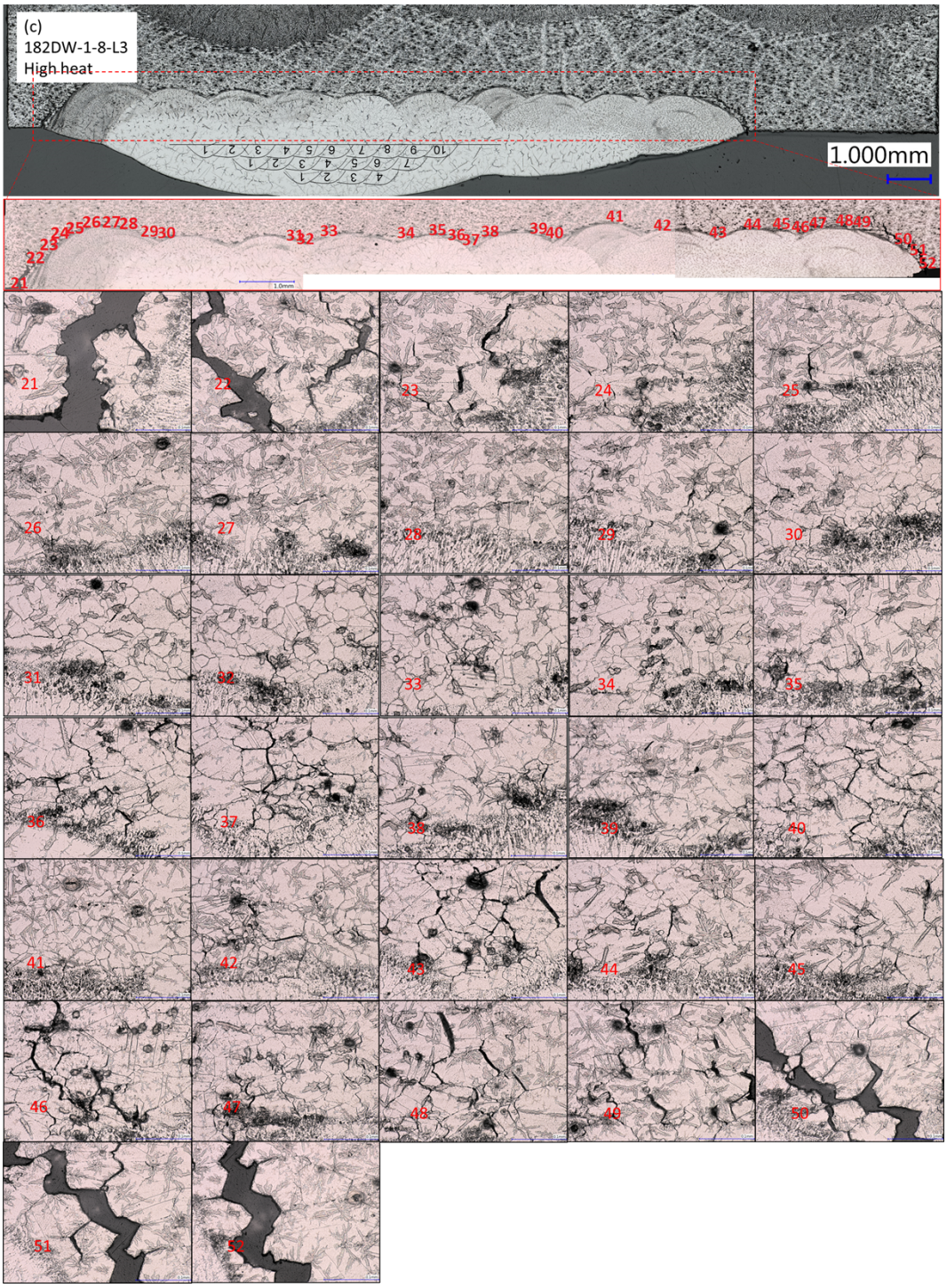
(c)
182DW-1-8-L3
High heat
1.000mm

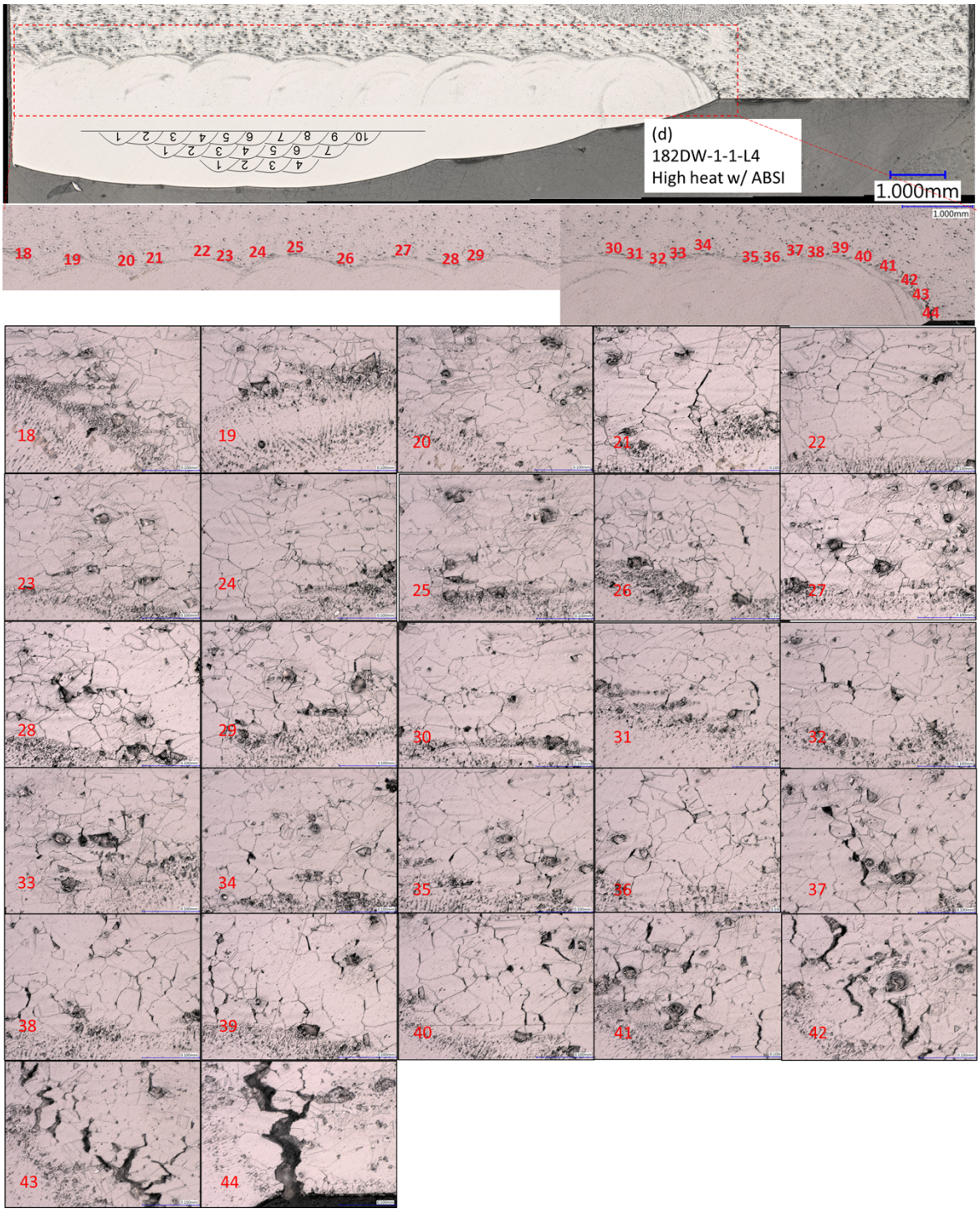

Figure 9 Cross-section views of LW cladding of alloy 182 with 14 wppm B with different welding conditions: (a) low heat input without ABSI (weld microstructure side); (b) low heat input with ABSI (weld microstructure side); (c) high heat input without ABSI; (d) high heat input with ABSI.

4. SUMMARY

This report describes the research activities conducted in FY 2023 on post-weld evaluation and characterization of the quality and properties of welds made on irradiated Ni-base alloy 182 (with boron concentration up to 15 wppm) by the advanced laser repair welding technology developed under the DOE Light Water Reactor Sustainability Program and EPRI LTO program. The research represents a major progress in repair welding of highly irradiated helium containing reactor internals and its feasibility to use the ABSI-LW technology developed in this program. The major findings include:

1. With boron concentration up to 15 wppm and the laser weld clads produced on the original base metals, no major cracks were observed in most of the HAZ except for the weld toe regions, suggesting a refined laser parameter is required at the beginning and end of the pass sequences.

2. Grain boundary degradation was observed through the HAZ. Application of ABSI seems helpful to reduce the tendency of grain boundary degradation.

3. The pre-existing weld microstructure has a large impact on HeIC possibly due to boron segregation during the welding performed prior to irradiation. More studies are required to further investigate the influence and seek the mitigation strategy.

In summary, these findings from this study suggest pathways to further refine and optimize the laser welding parameters for successful repair welding of nuclear reactor internals having helium levels much higher than what can be addressed by current weld repair technologies.

5. REFERNECES

Asano, K., S. Nishimura, Y. Saito, H. Sakamoto, Y. Yamada, T. Kato and T. Hashimoto (1999). "Weldability of neutron irradiated austenitic stainless steels." Journal of Nuclear Materials **264**(1-2): 1-9.

EPRI (2015). BWRVIP-97, Revision 1: BWR Vessel and Internals Project, Guidelines for Performing Weld Repairs to Irradiated BWR Internals, EPRI.

Feng, Z., R. G. Miller, N. Cetiner, X. Hu, S. Clark, G. Frederick and B. Sutton (2017). Report Summarizing the Status of Second Round Irradiation Experiments and Assessment of Materials Available for Testing Advanced Welding (M3LW-17OR0406013). DOE Light Water Reactor Sustainability Program, Oak Ridge National Laboratory.

Feng, Z., R. G. Miller, J. Chen, M. Gussev, X. Hu, W. Tang, G. Frederick, J. Tatman and B. Sutton (2019). Recent Technological Advances in Welding Irradiated Helium Containing Austenitic Steel (M3LW-19OR0406015). DOE Light Water Reactor Sustainability Program, Oak Ridge National Laboratory.

Feng, Z., R. G. Miller, J. Chen, W. Tang, S. Clark, B. Gibson, M. Vance, G. Frederick, J. Tatman and B. Sutton (2017). Development of Welding Parameters for Irradiated Materials (M2LW-17OR0406014). DOE Light Water Reactor Sustainability Program, Oak Ridge National Laboratory.

Feng, Z., W. Tang, R. G. Miller, J. Chen, S. Clark, B. Gibson, G. Frederick, J. Tatman and B. Sutton (2018). Complete Report on Development of Weld Repair Technology (M2LW-18OR0406014). DOE Light Water Reactor Sustainability Program, Oak Ridge National Laboratory.

Feng, Z., W. Tang, R. G. Miller, J. Chen, M. Gussev, S. Clark, G. Frederick, J. Tatman and B. Sutton (2019). Develop Parameters and Characterize the Quality of Friction Stir and Laser Weld-Repaired, Irradiated Structural Materials Representative of Extended Reactor Service Life (M2LW-19OR0406014). DOE Light Water Reactor Sustainability Program, Oak Ridge National Laboratory.

Feng, Z. and G. M. Wilkowski (2002). Repair Welding of Irradiated Materials - Modeling of Helium Bubble Distributions for Determining Crack-Free Welding Procedures. 10th International Conference on Nuclear Engineering, ASME.

Feng, Z., K. Wolfe and E. Willis (2009). BWRVIP-228: BWR Vessel and Internals Project: A Computational Modeling Tool for Welding Repair of Irradiated Materials, EPRI.

JNES (2004). FY2003 Nuclear Power Plant Maintenance Improvement Technology (PMT), Japan Nuclear Energy Safety Organization.

JNES (2004). FY2003 Safe Maintenance/Repair Welding Techniques for Nuclear Plant Irradiated Materails (WIM), Japan Nuclear Energy Safety Organization.

Kanne Jr., W. R. (1988). "Remote Reactor Repair, GTA weld cracking caused by entrapped helium." Welding Journal(8): 33-39.

Lin, H. T., M. L. Grossbeck and B. A. Chin (1990). "Cavity Microstructure and Kinetics During Gas Tungsten Arc Welding of Helium-Containing Stainless Steel." Metallurgical Transactions A **21A**(9): 2585-2596.

Willis, E. (2006). BWRVIP-151: BWR Vessle and Internals Project, Technical Basis for Resision to BWRVIP-97 Welding Guidelines, EPRI.

Chen, W., et al., (2001), "Effect of boron segregation at grain boundaries on heat-affected zone cracking in wrought INCONEL 718." Metallurgical and materials transactions A 32 (2001): 931-939

Chen, J., et al., "Suppression of Helium Induced Cracking in Laser Repair Welding of Highly Irradiated Stainless Steels." Journal of Nuclear Materials 556 (2021): 153206.